Experimental study of the effect of inclination angle on the thermal performance of heat pipe photovoltaic/thermal (PV/T) systems with wickless heat pipe and wire-meshed heat pipe

Mingke Hu [a], Renchun Zheng [b], Gang Pei *[, a], Yunyun Wang [c,a], Jing Li [a], Jie Ji [a]

[a] *Department of Thermal Science and Energy Engineering, University of Science and Technology of China, Hefei 230027, China*

[b] *Fujian Academy of Building Research, Fuzhou 350000, China*

[c] *Key Laboratory of Optoelectronic Devices and Systems of Ministry of Education and Guangdong Province, College of Optoelectronic Engineering, Shenzhen University, Shenzhen 518060, China*

*Corresponding author. Tel.: 0086-551-63601652. E-mail address: peigang@ustc.edu.cn.

Abstract

Two different heat pipe photovoltaic/thermal (PV/T) systems, namely, wickless heat pipe PV/T system and wire-meshed heat pipe PV/T system, were proposed. In this paper, the thermal performances of the two systems working on different inclination angles were experimentally investigated in an Enthalpy Difference Laboratory with a solar simulator. The thermal performance of the wire-meshed heat pipe is not as sensitive to the inclination angle as that of the wickless heat pipe. The wickless heat pipe PV/T system is recommended at latitudes higher than 20°, whereas wire-meshed heat pipe PV/T system is suggested at latitudes lower than 20°. Moreover, the thermal performances of both PV/T collectors at an inclination angle of 40° were further investigated, in which case both heat pipes worked at optimum conditions. The thermal efficiency of the wickless heat pipe PV/T system and wire-meshed heat pipe PV/T system at zero reduced temperature was 52.8% and 51.5%, respectively.

KEYWORDS: *heat pipe; inclination angle; PV/T; solar energy; thermal efficiency*

1. Introduction

The exhaustion of conventional energy resources and the serious problems caused by environment pollution are the main reasons for using various sustainable green energy resources. Solar energy is one of the most abundant renewable energy sources and emits energy at a rate of 3.8×10^{23} kW, of which approximately 1.8×10^{14} kW is diverted to the Earth [1]. Integrating solar energy utilization technologies in buildings is becoming widely practiced [2–6]. Efficiently utilizing solar energy in a limited area in a building facçade has become significant concern. Structurally, a flat-plate solar collector can be installed easily in buildings [4, 7]. In various applications of flat-plate solar collector, the hybrid PV/T technology integrates photovoltaic and photo-thermal components and generates electrical and thermal energy simultaneously, thus increasing the comprehensive utilization efficiency of solar irradiance. Cooling liquid can reduce the working temperature of PV cells and increase the photovoltaic efficiency of the system [8–10]. Basically, water-cooled PV/T systems could lower the temperature of PV cells, thus increasing photovoltaic efficiency than air-cooled PV/T systems [11]. However, traditional water-cooled PV/T systems have drawbacks. The working fluid of water-cooled PV/T systems freezes easily in frozen areas or locations with cold weather conditions. The solar panel tends to corrode after being utilized for an extended period of time. The application of a heat pipe PV/T system successfully addressed the problems associated with traditional water cooled PV/T systems [12]. Moreover, the temperature gradient along the length direction of the heat pipe is negligible because of phase change heat transfer in the evaporation of the heat pipe. Thus, the temperature distribution of the solar panel is relatively uniform, and photovoltaic efficiency is enhanced [13].

Inclination angle and filling ratio are two key factors that affect the thermal performance of a heat pipe [14, 15]. Some researchers studied the heat transfer performance of two-phase closed thermosyphon with different inclination angles under various working conditions [14–20]. Basically, the heat transfer rate is insensitive to the inclination angle when the latter changes from 20° to 75° for the gravity heat pipe, whereas the heat transfer rate decreases abruptly when the inclination angle

changes from 20° to 0°. Generally, the solar panel of a flat-plate collector is always placed at an inclination angle. For traditional water cooled PV/T systems, the pump drives water directly through the copper pipes of the solar panel and the heat transfer rate is slightly affected by gravity. Thus, the collector is usually mounted at an inclination angle that corresponds to the local latitude to maximize the received annual total solar irradiance. However, the inclination angle in a heat pipe PV/T system significantly affects the received annual total solar irradiance and the thermal performance of the heat pipe. Thus, considering both factors is necessary in designing the optimum inclination angle of the heat pipe PV/T system.

To the authors' knowledge, most previous researches focused only on the thermal performance of the heat pipe or discussed the other novel structures of the heat pipe PV/T system [21, 22]. A few studies discuss the effect of inclination angle on the thermal performance of the heat pipe PV/T system. Furthermore, outdoor experimental studies have their own limitations because outdoor environmental conditions, such as solar irradiance, ambient temperature, and wind velocity, change constantly. Thus, setting the inclination angle as the only variable is difficult in examining its effect on the thermal performance of the heat pipe PV/T system in outdoor conditions. In this study, we selected two types of heat pipes, namely, type A: wickless heat pipe and type B: wire-meshed heat pipe (the wire-mesh functions as the wick structure), as the main research subjects of two heat pipe PV/T systems. Our experiment was carried out in an Enthalpy Difference Laboratory (EDL) with a solar simulator to ensure that the heat pipe PV/T systems would operate in a stable external environment. Hence, the thermal performances of the two different heat pipe PV/T systems working on different inclination angles were experimentally investigated.

2. Theoretical model of the inclined heat pipe

Basically the heat pipes were placed with an inclination angle in the research area of heat pipe PV/T system. Additionally, the heat flux in the heat pipe PV/T system is far below the heat transfer limits and the evaporating section is under mild boiling state. Thus the heat transfer performance in

the evaporating section is almost irrelative with the inclination angle. What is more, the performance of the wire-meshed heat pipe is also insensitive to the inclination angle due to the capillary force of the wire-mesh. Accordingly, in this section we only focus on the effect of the inclination angle on the performance of the condensing section of the wickless heat pipe.

Figure 1 shows the free-body diagram of the condensing section of the inclined wickless heat pipe, where θ is the inclination angle with respect to horizontal (°), Φ is the azimuthal angle (°). Equations (1) and (2) are the governing equations of momentum for the condensate film in cylindrical coordinates [23]:

$$\mu_{\mathrm{l}} \frac{\partial^2 v_x}{\partial y^2} + \left(\rho_{\mathrm{l}} - \rho_{\mathrm{g}}\right) g \sin\phi \cos\theta = 0 \tag{1}$$

$$\mu_{\mathrm{l}} \frac{\partial^2 v_z}{\partial y^2} + \left(\rho_{\mathrm{l}} - \rho_{\mathrm{g}}\right) g \sin\theta = 0 \tag{2}$$

where μ_{l} is the dynamic viscosity (N·s/m^2), v_x and v_z are the velocity components of the condensate liquid along x and z direction (m/s), ρ_{l} and ρ_{g} are the densities of the working liquid and vapor (kg/m^3). These equations are subjected to several boundary conditions as follows:

$$v_x = v_z = 0 \ , \quad y = 0 \tag{3}$$

$$\frac{\partial v_x}{\partial y} = \frac{\partial v_z}{\partial y} = 0 \ , \quad y = \delta \tag{4}$$

where δ is the condensate film thickness (m).

Based on the above equations, the velocity distribution of the condensate film can be express as：

$$v_x = -\frac{\left(\rho_{\mathrm{l}} - \rho_{\mathrm{g}}\right) g \sin\phi \cos\theta}{2\mu_{\mathrm{l}}} y^2 + \frac{\left(\rho_{\mathrm{l}} - \rho_{\mathrm{g}}\right) g \sin\phi \cos\theta}{\mu_{\mathrm{l}}} y\delta \tag{5}$$

$$v_z = -\frac{\left(\rho_{\mathrm{l}} - \rho_{\mathrm{g}}\right) g \sin\theta}{2\mu_{\mathrm{l}}} y^2 + \frac{\left(\rho_{\mathrm{l}} - \rho_{\mathrm{g}}\right) g \sin\theta}{\mu_{\mathrm{l}}} y\delta \tag{6}$$

Equations (7) to (9) are the governing equations of energy for the condensate film in cylindrical coordinates:

$$h_{\mathrm{l}}(T_{\mathrm{s}}-T_{\mathrm{w}})dxdz=h_{\mathrm{fg}}d\dot{M} \tag{7}$$

$$d\dot{M}=d\dot{M}_{x}+d\dot{M}_{z}=\frac{\partial}{R\partial\phi}(\rho v_{x}\delta Rd\phi dz)+\frac{\partial}{\partial z}(\rho v_{z}\delta Rd\phi dz) \tag{8}$$

$$h_{\mathrm{l}}=\frac{k_{\mathrm{l}}}{\delta} \tag{9}$$

where h_{l} is the convective heat-transfer coefficient (W/m^2·K), h_{fg} is latent heat of vaporization (kJ/kg), $d\dot{M}$ is the increment in condensate mass flow rate through the control volume (kg/s), R is inner radius of the condensing section (m), k_{l} is the thermal conductivity of the condensate film (W/m·K).

Combining equations (5), (6) and (8), the condensate film thickness δ can be express as:

$$\frac{1}{3}\delta^{4}\cos\phi\cos\theta+\delta^{3}\cos\theta\sin\phi\frac{\partial\delta}{\partial\phi}+R\delta^{3}\frac{\partial\delta}{\partial z}=\frac{\mu_{\mathrm{l}}Rk_{\mathrm{l}}\left(T_{\mathrm{s}}-T_{\mathrm{w}}\right)}{\rho_{\mathrm{l}}\left(\rho_{\mathrm{l}}-\rho_{\mathrm{g}}\right)gh_{\mathrm{fg}}} \tag{10}$$

Meshing the condensing section by two dimensional grids and the condensate film thickness of each grid node could be obtained. Then the convective heat-transfer coefficient of each grid node can be calculated by equation (9). The average heat-transfer coefficient of the condensing section can finally be obtained by averaging the heat-transfer coefficient values of all the grid nodes:

$$\bar{h}=\frac{1}{\mathrm{M}\cdot\mathrm{N}}\sum h_{\mathrm{l}} \tag{11}$$

where M and N are the grid nodes in the circumferential direction and axial direction, respectively.

The thermal resistance of the condensing section can be written as:

$$R=\frac{1}{\bar{h}A} \tag{12}$$

where A is the heat transfer area of the condensing section (m^2).

3. Description of the heat pipe PV/T collectors and the experimental set-up

3.1 Description of the heat pipe PV/T collectors

To study the thermal performance of the heat pipe PV/T system, we designed two different types of heat pipe PV/T collectors, namely, wickless heat pipe PV/T collector and wire-meshed heat pipe

PV/T collector. The only difference between these two collectors is the inner structure of the heat pipe (see Fig.2). The collectors are composed of a glass cover, mono-crystalline silicon cells, an aluminum plate, a cooling water pipe, and an insulation layer. The structure of a heat pipe PV/T collector is presented in Fig. 3. A piece of aluminum plate with an area of 1270 mm × 780 mm and a thickness of 1.16 mm was selected as the base panel. Nine heat pipes with dimensions of $\phi 8 \times 1 \times 1300$ mm for the evaporating section and $\phi 24 \times 1 \times 90$ mm for the condensing section were welded at the back of the aluminum plate using a laser welding machine. The condensing section of each heat pipe was inserted into a copper sheathing, which was implanted through the cooling water pipe radially. The length between the two adjacent heat pipes was 80 mm. A section of the heat pipe PV/T collector is depicted in Fig. 4. Seventy-two pieces of small PV cells (mono-crystalline silicon) were laminated to the surface of the aluminum plate. A layer of black tedlar–polyester–tedlar (TPT) was placed between the PV cells and aluminum plate; this layer plays a role in the electrical insulation of PV cells and enhances the absorption of solar irradiance. The aperture area of the collector is 0.99 m^2, and the cell area is 0.56 m^2. A low-iron tempered and textured glass plate was installed anterior to the PV cells as the upper glazing for the collector, thereby permitting sunlight injection and preventing thermal loss and the entry of dust particles and rain. The air gap between the glass cover and the PV plate was 40 mm. A thermal insulation layer with a thickness of 50 mm was placed behind the aluminum plate.

When solar irradiance passes through the glass cover and penetrates the PV layer, most of the solar irradiance is absorbed by the black TPT layer and PV cells. Some of the absorbed irradiance is converted to electricity, and the rest is eventually converted to heat energy. The heat energy is conducted along the aluminum plate to the evaporating section of the heat pipes. The heat pipes transfer this energy through their condensing sections to the flowing water through the cooling water pipe.

3.2 Experimental set-up

To study the thermal performance of the two heat pipe PV/T collectors, two experimental systems (system A: with wickless heat pipe and system B: with wire-meshed heat pipe) were set up in an EDL with a solar simulator. The configuration diagram of the experimental setup of the heat pipe PV/T system is shown in Fig. 5. This system mainly consists of a heat pipe PV/T collector, circulation pump, water flowmeter, water tank (120 L), solar photovoltaic controller, an electric power sensor, accumulator, and several valves.

The research subject of this paper is the effect of inclination angle (θ) on the thermal performance of the two heat pipe PV/T systems. Thus, accurate results would be obtained if the other parameters, except the inclination angle, were fixed. Outdoor experimental studies have their own limitations because outdoor environmental conditions, such as ambient temperature and humidity, solar irradiance, and wind velocity, change constantly. Thus, setting the inclination angle as the only variable is difficult when studying its effect on the thermal performance of the heat pipe PV/T system in outdoor conditions. Hence, our experiments were carried out in an EDL with a solar simulator to ensure that the heat pipe PV/T systems operate in a stable external environment.

The EDL (Fig. 6) was designed and constructed by Hefei General Machinery Research Institute, and the temperature and humidity in the EDL can be controlled accurately. The dry-bulb temperature could be regulated from -15 °C to 50 °C with an accuracy of ±0.2 °C, and the ambient relative humidity could be adjusted from 20% to 90%. The solar simulator could offer stable solar irradiation and inclination angles from 0° to 90°. The heterogeneity and instability of the solar simulator are less than 5%, and the spectrum distribution satisfies the Chinese National Class B standard. The adjustable range of the irradiance is between 200 and 1200 W/m^2 with a luminous area of 4 m^2. In this study, the solar simulator was parallel to the heat pipe PV/T collectors.

A list of experimental testing and monitoring devices is provided in Table 1. The solar irradiance from the solar simulator was measured by using a TBQ-2A Pyranometer. The flow rate of the circulating water was determined by using a LXS 20C water flowmeter. The electric output was

measured by using a WBI021S91 power sensor, and the solar photovoltaic controller was SD4815 style. Copper–constantan thermocouples and platinum resistors were employed in this study to measure the temperature. Five thermocouples were adhered to the back of the absorber plate evenly along the axis. Five other thermocouples were arranged in the water tank at different altitudes. The inlet and outlet water temperatures were measured by using two platinum resistors separately. All data were recorded by using an Agilent data acquisition instrument with an interval of 30 s.

4. Performance evaluation of the heat pipe PV/T system and the experimental methods

4.1 Performance evaluation of the heat pipe PV/T system

We evaluated the performance of the two heat pipe PV/T systems on the basis of the data acquired by the Agilent data acquisition instrument.

The instantaneous electrical efficiency of the system is given by

$$\eta_{pv} = \frac{E_{pv}}{\xi A_c G} = \frac{UI}{\xi A_c G} \tag{13}$$

where E_{pv} is the instantaneous electrical power of the system (W), ξ is the packing factor of the PV cells, A_c is the aperture area of the collector (m^2), G is the incident solar irradiance per square meter (W/m^2), and U and I are the output voltage (V) and output current (A) of the system, respectively.

The average electrical efficiency of the system is given by

$$\eta_{pv} = \frac{E_{pv}\Delta t}{\xi H_t} \tag{14}$$

where Δt is the total testing time (s) and H_t is the total solar irradiance during the testing time (J).

The instantaneous thermal efficiency of a PV/T collector can be defined as the heat gain of the working fluid between the outlet and inlet of collector divided by incident solar irradiance expressed as

$$\eta_{th} = \frac{\dot{m} c_w (T_{out} - T_{in})}{G A_c} \tag{15}$$

where $\dot{m}$ is the mass flow rate of circulating water (kg/s), c_w is the specific heat capacity of water [J/(kg·K)], and T_{in} and T_{out} are the water temperatures at the inlet and outlet of the collector (K), respectively.

The Hottel-Whillier model is applied to eliminate the effect of variation of solar irradiance and temperature difference between ambient and water at the inlet of the collector and obtain general conclusions. The heat gain of the PV/T collector can be expressed as [24]

$$Q_u = A_c[GF_R(\tau\alpha)_e - F_R U_L(T_{in} - T_a)] \tag{16}$$

where F_R is the heat removal factor of the collector, $(\tau\alpha)_e$ is the effective transmittance–absorptance product, U_L is the energy loss coefficient of collector (K·m^2/W), and T_a is the ambient temperature (K).

Thus, the instantaneous thermal efficiencies of the collector can be plotted as a function of the reduced temperature, which is expressed as [25]

$$\eta_{th} = F_R(\tau\alpha)_e - F_R U_L \frac{T_{in} - T_a}{G} \tag{17}$$

where intercept $F_R(\tau\alpha)_e$ and slope $F_R U_L$ represent the thermal efficiency of the collector at zero reduced temperature and energy loss of the collector, respectively.

The average thermal efficiency of the system depends on the total solar irradiance of the aperture area, initial and final water temperatures in water tank, and mass of water in the water tank. The average thermal efficiency can be written as

$$\overline{\eta_{th}} = \frac{Q_w}{H_t} = \frac{c_w m(T_{final} - T_{initial})}{H_t} \tag{18}$$

where Q_w is the total heat gain of water in the water tank (J), m is the mass of water in the water tank (kg), and $T_{initial}$ and T_{final} are the initial and final water temperatures in water tank (K), respectively. The water temperature in the water tank is the average temperature of the five thermocouples in the water tank

$$T_w = \frac{\sum_1^5 T_i}{5} \tag{19}$$

where T_i is the measured value of water temperature in the water tank as measured by the thermocouple.

According to the theory of error propagation, the relative error (RE) of the dependent variable y can be calculated as follows [26]:

$$RE = \frac{dy}{y} = \frac{\partial f}{\partial x_1}\frac{dx_1}{y} + \frac{\partial f}{\partial x_2}\frac{dx_2}{y} + \cdots + \frac{\partial f}{\partial x_n}\frac{dx_n}{y} \tag{20}$$

$$y = f(x_1, x_2, \cdots, x_n) \tag{21}$$

where x_i, (i = 1, …, n) is the variable of the dependent variable y, $\partial f / \partial x$ is the error transferring coefficient of the variables.

The experimental relative mean error (RME) during the test period can be expressed as:

$$RME = \frac{\sum_1^N |RE|}{N} \tag{22}$$

4.3 Experimental methods

The two different heat pipe PV/T collectors were mounted directly under the solar simulator and always positioned parallel to the plane of the solar simulator. We set seven different inclination angles of the heat pipe PV/T collectors and solar simulator (i.e., 10°, 20°, 30°, 40°, 50°, 60°, and 70°) to evaluate the performance of the two heat pipe PV/T systems under different inclination angles. The ambient temperature was fixed at 25 ℃. Before each test, the water tank was filled with water at 25 ℃. The solar irradiance from the solar simulator was stabilized at 650 W, and the flow rate of circulating water was maintained at 0.033 kg/s. Each experiment ended when the water temperature in the water tank exceeded 40 ℃.

5. Results and discussions

5.1 Thermal resistance in the condensing section

In terms of the heat pipe PV/T collectors of this paper, the operation temperature of the working liquid is set as 32℃, and the temperature difference between the liquid and wall is set as 3℃. On basis of the theoretical analysis in section 2, we can calculate the heat transfer power in the condensing section of the wickless heat pipe under different inclination angles. As is shown in Fig. 7, the thermal resistance in the condensing section of the wickless heat pipe is about 0.027 K/W when the inclination angle is 10°. Then the thermal resistance decreases sharply to approximately 0.014 K/W at an inclination angle of 20°. A gradual increase was seen in the next two inclination angles, with the thermal resistance bottoming out at almost 0.011 K/W at an inclination angle of 40°. This value then increases slightly between the inclination angles of 40° and 70°, and ends at approximately 0.012 K/W at an inclination angle of 70°. We can learn from Fig. 7 that the thermal performance of wickless heat pipe is sensitive to the inclination angle when the latter is lower than 20°, which is because the gravity component along the axial direction is too small to let the working fluid in the condensing section flow back to the evaporating section completely, thereby the thermal resistance remains at relatively high values and the heat pipe works at relatively poor condition.

5.1 Photo-thermal performance

The variation of the average heating power within every 30 min and the water temperature in the water tank under seven inclination angles of the heat pipe PV/T collectors are shown in Fig. 8. The figure indicates that the average heating power of both systems reduced with time under any of the seven inclination angles. Moreover, the average heating power of system A (wickless heat pipe PV/T system) was always slightly higher than that of system B (wire-meshed heat pipe PV/T system) except that with an inclination angle of 10°, under which the average heating power of system A was significantly lower than that of system B. This result indicates that the wickless heat pipes in system A did not function properly under an inclination angle of 10°.

Figure 8 demonstrates that, under any of the seven inclination angles, the average water temperatures in the water tank of both systems A and B increase steadily with time. Solar irradiation

and ambient temperature were fixed during the test. Thus, the conductive and convective heat loss of the systems increased with the water temperature in the water tank and circulation loop, thus reducing heating power. Under inclination angles of 20° to 70°, the average water temperature in the water tank of the two systems exhibited almost the same increasing velocity. The final water temperatures in the water tank of system A were approximately 0.5 °C to 2 °C higher than those of system B. This finding indicates that the thermal performance of systems A and B or the thermal performance of wickless heat pipe and wire-meshed heat pipe was not significantly different under these conditions. However, at an inclination angle of 10°, a significant difference in the variation of the average water temperature in the water tank was observed between the two systems. The increase in velocity of the average water temperature in the water tank of system A was significantly lower than that of system B. At the end of the experiment, the water tank temperature of system A increased by only approximately 3.8 °C, whereas that of system B increased by 16.5 °C. This result is due to the significant difference of the average heating power between systems A and B under an inclination angle of 10°.

The thermal efficiency of systems A and B is compared in Fig. 9. The thermal efficiency of systems A shows the reversing trend to the thermal resistance in the condensing section of wickless heat pipe (see Fig. 7). When the inclination angle is 10°, the thermal efficiency of system A is extremely low (roughly 10%). The thermal efficiency increases rapidly to approximately 43% at an inclination angle of 20°. A gradual increase was observed in the next two inclination angles, with the thermal efficiency peaking slightly higher than 50% at an inclination angle of 40°. The thermal efficiency of system A decreases slightly between the inclination angles of 40° and 70°, and ends at approximately 48% at an inclination angle of 70°. By contrast, the thermal efficiency of system B is always higher than 40% under any of the seven inclination angles. Specifically, the thermal efficiency of system B is always slightly lower than that of system A under inclination angles of 20°

to 70°. However, the thermal efficiency of system B remains stable over 40% at an inclination angle of 10°. The thermal efficiency of system B also reaches its peak at an inclination angle of 40°.

On the basis of the testing and analysis results, we can conclude that the thermal performance of wickless heat pipe in system A is sensitive to the inclination angle. Theoretically, the boiling modes of the evaporating section, condensate film distribution, and return flow velocity of the working fluid are all highly correlated with the inclination angle. We also determine that the working fluid of the wickless heat pipe in system A works at the optimum condition at an inclination angle of 40°, thereby demonstrating that the thermal resistance of wickless heat pipe is minimal in this case. When the inclination angle is higher or lower than 40°, heat transfer would deteriorate because of the force condition of the working fluid. The axial component of gravity is too small to fully drive the working fluid in the condensing section back to the evaporating section when the inclination angle is lower than 40°, particularly when the inclination angle is below 20°, which results in the larger thermal resistance of the wickless heat pipe and worsens heat transfer performance. In addition, as the inclination angle changing from 40° to 70°, the vapor ascended from the evaporating section to the condensing section is partly blocked by the interfacial shear stress of the return flow of the working fluid, which also leads to worse heat transfer performance. By contrast, the thermal performance of the wire-meshed heat pipe in system B is not sensitive to the inclination angle unlike the wickless heat pipe in system A. The thermal resistance of the inner wall of the wire-meshed heat pipe is slightly higher than that of the wickless heat pipe because of the wire-mesh, which could explain why the thermal efficiency of system B is marginally lower than that of system A when the inclination angle is higher than 20°. However, when the inclination angle is lower than 20°, the wire-meshed heat pipe in system B can still operate efficiently although the axial component of gravity is small because of the capillary force of the wire-mesh. Moreover, the thermal efficiency also experiences a gradual decrease as the inclination angle changing from 40° to 70° due to the gradual increase of the interfacial shear stress of the return flow. Accordingly, the wickless heat pipe PV/T

system can be employed at latitudes higher than 20°, whereas the wire-meshed heat pipe PV/T system can be used at latitudes lower than 20° considering the relationship between the inclination angle of the PV/T collector and local latitude.

Systems A and B both exhibit the highest thermal efficiency at an inclination angle of 40°. Thus, we further examined the instantaneous thermal efficiency of both PV/T collectors A and B at an inclination angle of 40°. The curves of η_{th} against $(T_{in}\text{-}T_a)/G$ are shown in Fig. 10. According to Equation (5), the thermal efficiencies of the two collectors can be expressed with regression lines

$$\eta_{th,A} = 0.528 - 6.83\frac{T_{in} - T_a}{G} \tag{8}$$

$$\eta_{th,B} = 0.515 - 7.49\frac{T_{in} - T_a}{G} \tag{9}$$

Figure 10 indicates that the thermal efficiency of collector A is always marginally higher than that of collector B. In addition, the thermal efficiency of collectors A and B at zero reduced temperature was 52.8% and 51.5%, respectively. As the $(T_{in}\text{-}T_a)/G$ value increased, the thermal efficiency of both collectors decreased gradually with slopes at -6.83 and -7.49, respectively, thereby demonstrating that the reduction in velocity of the thermal efficiency of collector A is lower than that of collector B.

The thermal efficiency at the zero reduced temperature was slightly higher than that in our previous work on a heat pipe PV/T collector [11]. The results exhibit better linearity and less error (R_A^2=0.995, R_B^2=0.996) compared with the results in Reference [11] because the experiments of this study are carried out in the EDL where the ambient temperature, solar irradiance, wind velocity, and humidity were nearly constant throughout the test period. By contrast, the experiments of Reference [11] were conducted outside a laboratory where these parameters change constantly.

5.2 Photovoltaic performance

Both collectors were mounted directly under the solar simulator and always positioned parallel to the plane of the solar simulator. Thus, the electric powers of both collectors show no significant

difference among the different inclination angles in this study. This finding indicates that the photovoltaic performance of the heat pipe PV/T collector is not correlated with the inclination angle of the heat pipe. However, Equation (1) indicates that the instantaneous photovoltaic efficiency of systems A and B was only approximately 6%, which is significantly lower than that in our previous work on a heat pipe PV/T system [11]. This outcome is due to the fact that the solar simulator in our experiments is at the B level according to the standard of International Electrical Commission (IEC). Its spectral distribution property differs from the AM1.5 solar spectrum to some extent. Specifically, a substantial part of the irradiance from the B level solar simulator is concentrated in the near-infrared regions other than the visible wavelengths where the optimum photovoltaic conversion efficiency occurs. In addition, the solar irradiance of each PV cell varies slightly because of the irradiation non-uniformity of the solar simulator. The PV cells in this study are connected in series. Thus, the output current of the PV/T collector is determined by the cell where solar irradiance is the lowest [27], which further reduces the photovoltaic efficiency of the collector. However, according to the standard of IEC, the B level solar simulator applied in our experiments is valid to investigate the thermal performance of the solar PV/T collector, which is the research emphasis of this study.

6. Conclusions

Two heat pipe PV/T systems, namely, wickless heat pipe PV/T system and wire-meshed heat pipe PV/T system, were proposed. In this paper, the thermal performances of the two systems operating on different inclination angles were experimentally investigated in an EDL with a solar simulator. The results are as follows:

(1) The thermal performance of the wickless heat pipe is sensitive to its inclination angle. When the inclination angle is below 20°, the thermal resistance of the wickless heat pipe is large. Thus, thermal performance is poor. The thermal performance of the wire-meshed heat pipe is not sensitive to the inclination angle unlike the wickless heat pipe because of the wire-mesh.

(2) Both the wickless heat pipe and wire-meshed heat pipe operate under the optimum condition

at an inclination angle of 40°. Likewise, the wickless heat pipe PV/T system and wire-meshed heat pipe PV/T system exhibit their highest thermal efficiencies at an inclination angle of 40°.

(3) At an inclination angle of 40°, the thermal efficiency of the wickless heat pipe PV/T collector and wire-meshed heat pipe PV/T collector at zero reduced temperature is 52.8% and 51.5%, respectively.

(4) The wickless heat pipe PV/T system may be employed at latitudes higher than 20°, whereas the wire-meshed heat pipe PV/T system can be used at latitudes lower than 20°. This general conclusion could also be extended to the application of heat pipe-solar heating collectors.

Acknowledgements

The study was sponsored by (1) the National Science Foundation of China (NSFC 51476159, 51178442, 51206154, and 51408578), (2) the Fundamental Research Funds for the Central Universities, and (3) Dongguan Innovative Research Team Program (No. 2014607101008).

References

[1] Thirugnanasambandam M, Iniyan S, Goic R, A review of solar thermal technologies, Renewable and Sustainable Energy Reviews 14 (2010) 312-322.

[2] Daniel Chemisanaa , Jesús López-Villadab, Alberto Coronas, et al, Building integration of concentrating systems for solar cooling applications, Applied Thermal Engineering 50 (2013) 1472-1479.

[3] Joshua Fong, Zaid Alwan, Modelling to predict future energy performance of solar thermal cooling systems for building applications in the North East of England, Applied Thermal Engineering 57 (2013) 81-89.

[4] Zhi Yu, Jie Ji, Wei Sun, et al. Chen. Experiment and prediction of hybrid solar air heating system applied on a solar demonstration building, Energy and Buildings 78 (2014) 59-65.

[5] J. Aman, D.S.-K. Ting, P. Henshaw, Residential solar air conditioning: Energy and exergy analyses of an ammonia-water absorption cooling system, Applied Thermal Engineering 62 (2014) 424-432.

[6] Sapfo Tsoutsou, Carlos Infante Ferreira, Jan Krieg, et al, Building integration of concentrating solar systems for heating applications, Applied Thermal Engineering 70 (2014) 647-654.

[7] Ibrahim Adnan, Fudholi Ahmad, Sopian Kamaruzzaman, et al. Efficiencies and improvement potential of building integrated photovoltaic thermal (BIPVT) system, Energy Conversion and Management 77 (2014) 527-534.

[8] Adnan Ibrahim, Mohd Yusof Othman, Mohd Hafidz Ruslan, et al. Recent advances in flat plate photovoltaic/thermal (PV/T) solar collectors, *Renewable and Sustainable Energy Reviews* 2011, 15:352-365.

[9] Aneta Hazi, Gheorghe Hazi, Roxana Grigore, Opportunity to use PVT systems for water heating in industry, Applied Thermal Engineering 63 (2014) 151-157.

[10] Bingzhi Zhang, , Jian Lv, Hongxing Yang, Performance analysis of a heat pipe PV/T system with different circulation tank capacities, Applied Thermal Engineering 87 (2015) 89-97.

[11] Jie Ji, Chao Guo, Wei Sun, et al, Experimental investigation of tri-functional photovoltaic/thermal solar collector, Energy Conversion and Management 88 (2014) 650-656.

[12] Pei Gang, Zhang Tao, Fu Huide, et al, Experimental study on a novel heat pipe-type photovoltaic/thermal system with and without glass cover, Journal of Green Energy 10(1) (2012) 72-89.

[13] Pei Gang, Fu Huide, Zhang Tao, et al, A numerical and experimengtal study on a heat pipe PV/T system, Solar Energy 85(5) (2011) 911-921.

[14] S. H. Noiea, M. R. Sarmasti Emamib, M. Khoshnoodib, Effect of Inclination Angle and Filling Ratio on Thermal Performance of a Two-Phase Closed Thermosyphon under Normal Operating Conditions, Heat Transfer Engineering 28(4) (2007) 365-371.

[15] Khazaee Iman, Hosseini Reza, Kianifar Ali, et al, Experimental Consideration and Correlation of Heat Transfer of a Two-Phase Closed Thermosyphon Due to The Inclination Angle, Filling Ratio, and Aspect Ratio, Journal of Enhanced Heat Transfer 18(1) (2011) 31-40.

[16] T.Payakaruk, P.Terdtoon, S.Ritthidech, Correlations to predict heat transfer characterristics of an inclined closed two-phase thermosyphon at normal operating conditions, Applied Thermal Engineering 20 (2000) 781-790.

[17] H.M.S.Hussein, M.A.Mohamad, A.S.Ei-Asfouri, Theoretical analysis of laminar-film condensation heat transfer inside inclined wickless heat pipes flat-plate solar collector Renewable Energy 23(3-4) (2001) 525-535.

[18] Runze Jia , Yichun Wang, Huining Shi, et al, Experimental and numerical study on the self-balancing heating performance of a thermosyphon during the process of oil production, Applied Thermal Engineering 73 (2014) 1270-1278.

[19] Mingyi Zhang, Yuanming Lai, Wansheng Pei, et al, Effect of Inclination Angle on the Heat Transfer Performance of a Two-Phase Closed Thermosyphon under Low-Temperature Conditions, Journal of Cold Regions Engineering 28(4) (2014) 04014007 (11 pp.).

[20] W. Srimuang, S. Rittidech, B. Bubphachot, Heat transfer characteristics of a vertical flat thermosyphon(VFT), Journal of Mechanical Science and Technology 23 (2009) 2548-2554.

[21] Xingxing Zhang, Xudong Zhao, Jingchun Shen, et al, Dynamic performance of a novel solar photovoltaic/loop-heat-pipe heat pump system, Applied Energy 114 (2014) 335-352.

[22] Zhang Longcan, Pei Gang, Zhang Tao, et al, A new photovoltaic solar-assisted loop heat pipe/heat-pump system, Journal of Chemical Industry and Engineering 65(8) (2014) 3228-3236.

[23] H.M.S. Hussein, M.A. Mohamad, A.S. El-Asfouri, Theoretical analysis of laminar-film condensation heat transfer inside inclined wickless heat pipes flat-plate solar collector, Renewable Energy 23 (2001) 525-535.

[24] J.A. Duffie, W.A. Beckman, Solar Engineering of Thermal Processes, 3rd ed. New York:

Wiley-Interscience; 2006.

[25] ANSI/ASHRAE 93 - Methods of testing to determine the thermal performance of solar collectors. New York: ASHRAE Inc.; 2010.

[26] Guiqiang Li, Gang Pei, Jie Ji, et al, Numerical and experimental study on a PV/T system with static miniature solar concentrator, Solar Energy 120 (2015) 565-574.

[27] Yunyun Wang, Gang Pei, Longcan Zhang, Effects of frame shadow on the PV character of a photovoltaic/thermal system, Applied Energy 130 (2014) 326-332.

Figure Captions

Fig. 1. The free-body diagram of the condensing section of the inclined wickless heat pipe.

Fig. 2. Inner structure of the two different types of heat pipe (a) wickless heat pipe (b) wire-meshed heat pipe.

Fig. 3. Heat pipe PV/T collector (a) schematic (b) photo.

Fig. 4. Section of the heat pipe PV/T collector.

Fig. 5. Configuration diagram of the experimental setup of the heat pipe PV/T system (a) schematic (b) photo.

Fig. 6. Schematic diagram of the Enthalpy Difference Laboratory (EDL).

Fig. 7. The heat transfer power in the condensing section of the wickless heat pipe under different inclination angles.

Fig. 8. Variation of water temperature in the water tank and heating power under different inclination angles of the heat pipe PV/T collectors.

Fig. 9. Thermal efficiency of system A (wickless heat pipe PV/T system) and system B (wire-meshed heat pipe PV/T system).

Fig. 10. Plot of instantaneous thermal efficiencies of the PV/T collectors at an inclination angle of 40°.

Table caption

Table 1 List of experimental testing and monitoring devices.

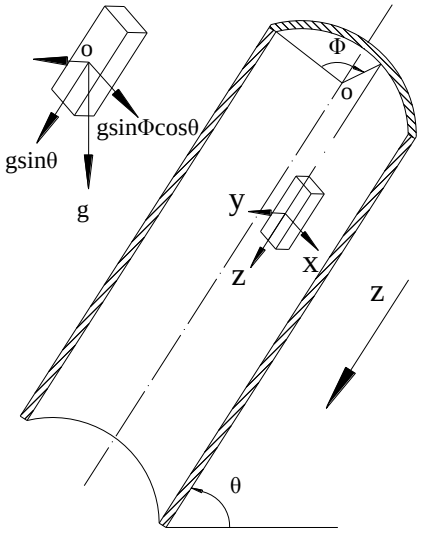

Fig. 1. The free-body diagram of the condensing section of the inclined wickless heat pipe.

(a) (b)

Fig. 2. Inner structure of the two different types of heat pipe

(a) wickless heat pipe (b) wire-meshed heat pipe.

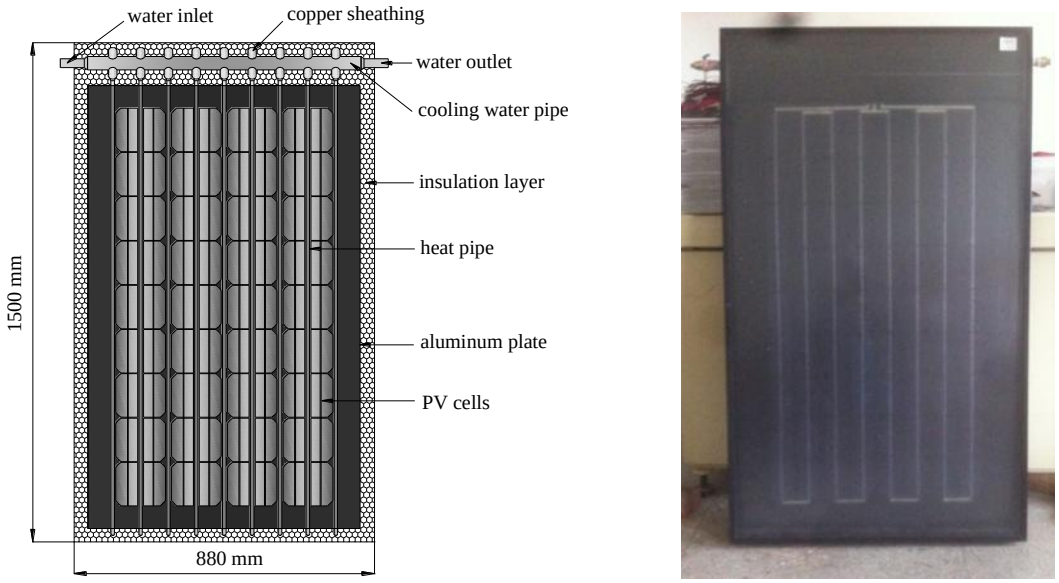

(a) (b)

Fig. 3. Heat pipe PV/T collector (a) schematic (b) photo.

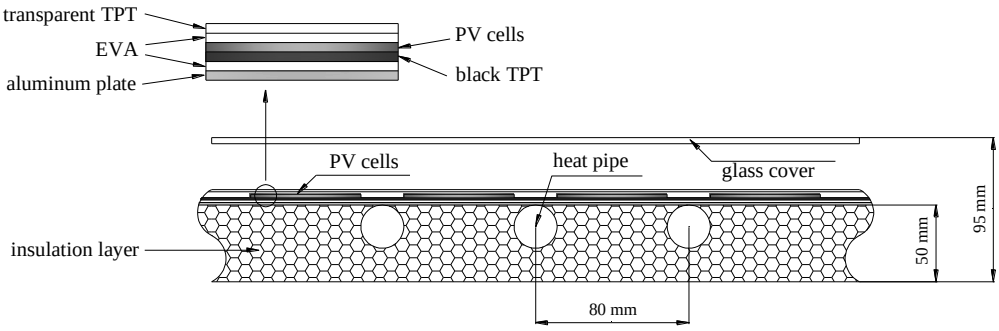

Fig. 4. Section of the heat pipe PV/T collector.

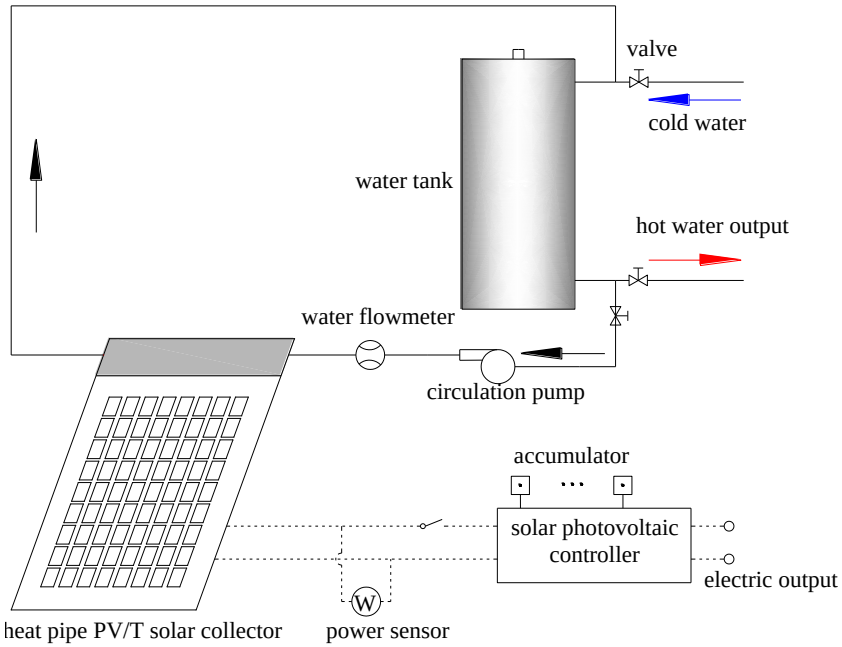

(a)

(b)

Fig. 5. Configuration diagram of the experimental setup of the heat pipe PV/T system

(a) schematic (b) photo.

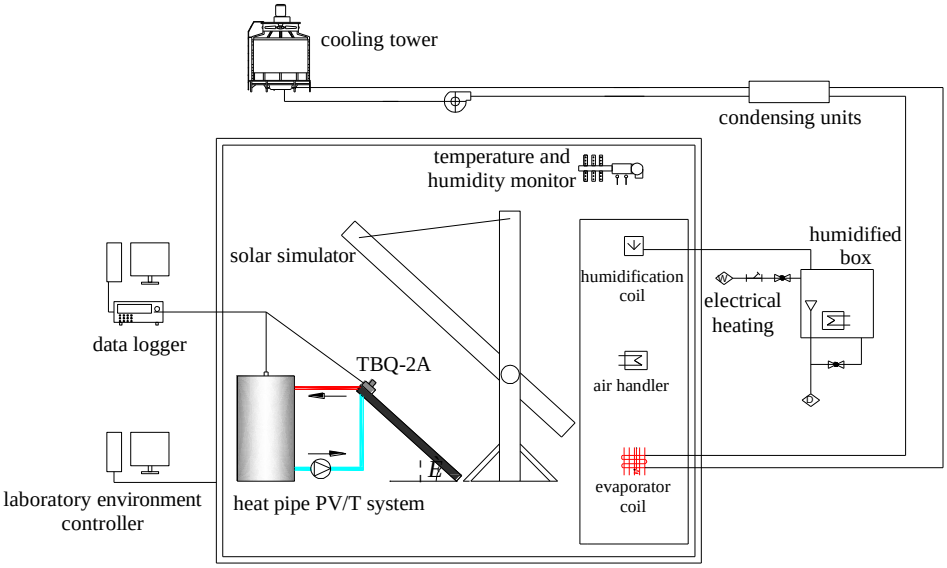

Fig. 6. Schematic diagram of the Enthalpy Difference Laboratory (EDL).

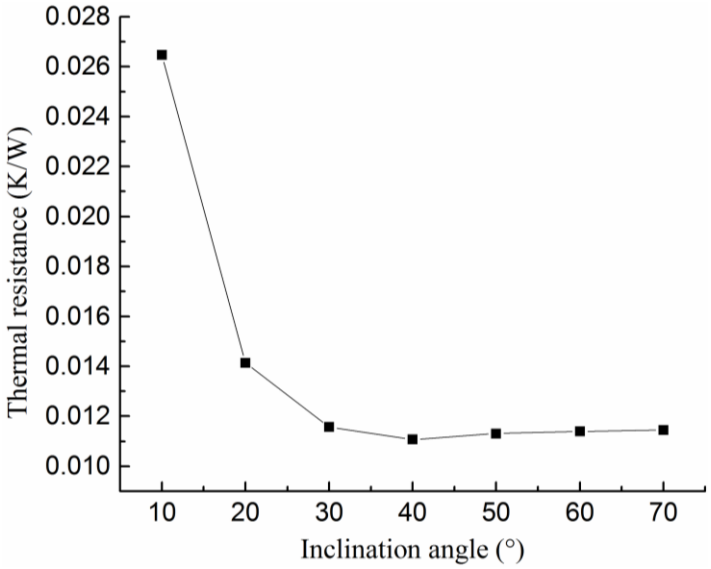

Fig. 7. The heat transfer power in the condensing section of the wickless heat pipe under different inclination angles.

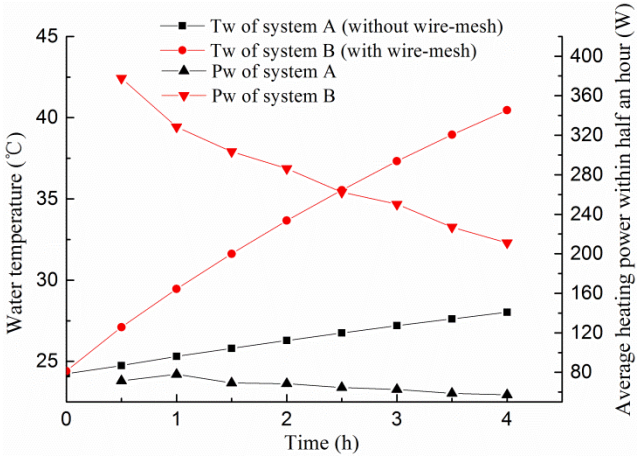

(a) inclination angle of 10°

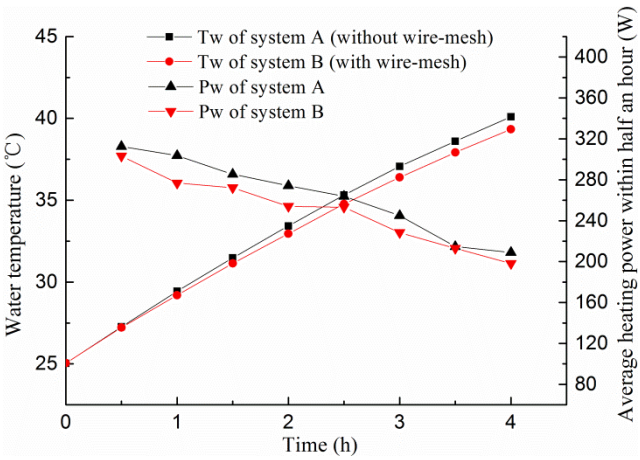

(b) inclination angle of 20°

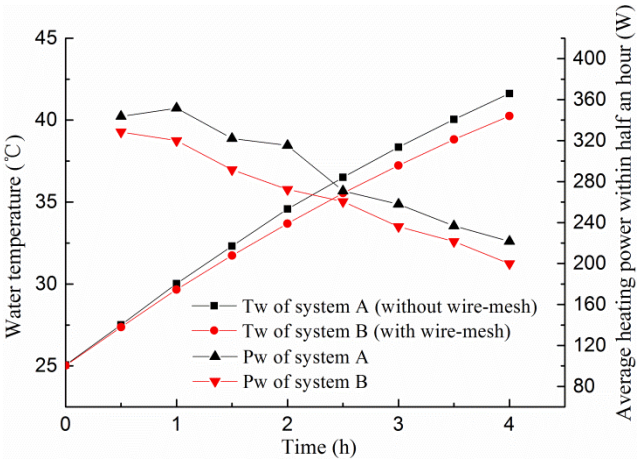

(c) inclination angle of 30°

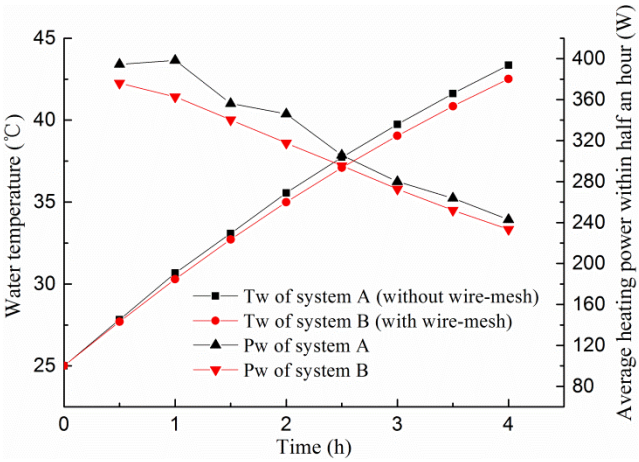

(d) inclination angle of 40°

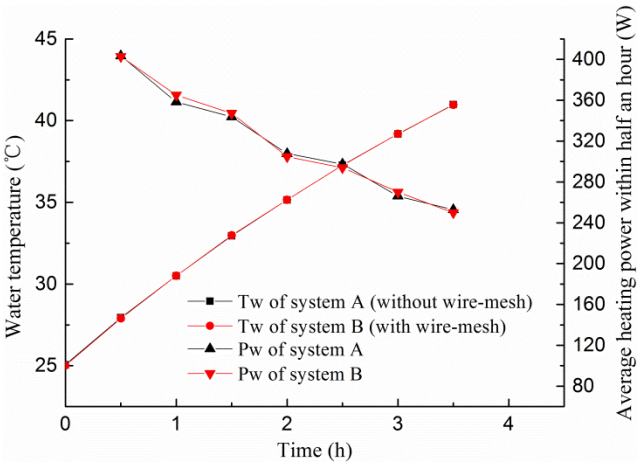

(e) inclination angle of 50°

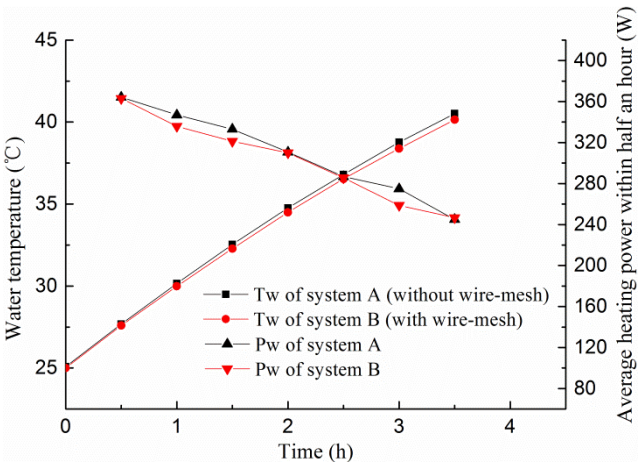

(f) inclination angle of 60°

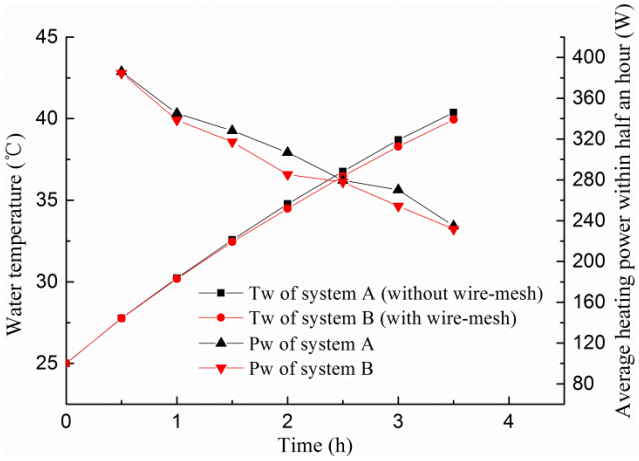

(g) inclination angle of 70°

Fig. 8. Variation of water temperature in the water tank and heating power under different inclination angles of the heat pipe PV/T collectors.

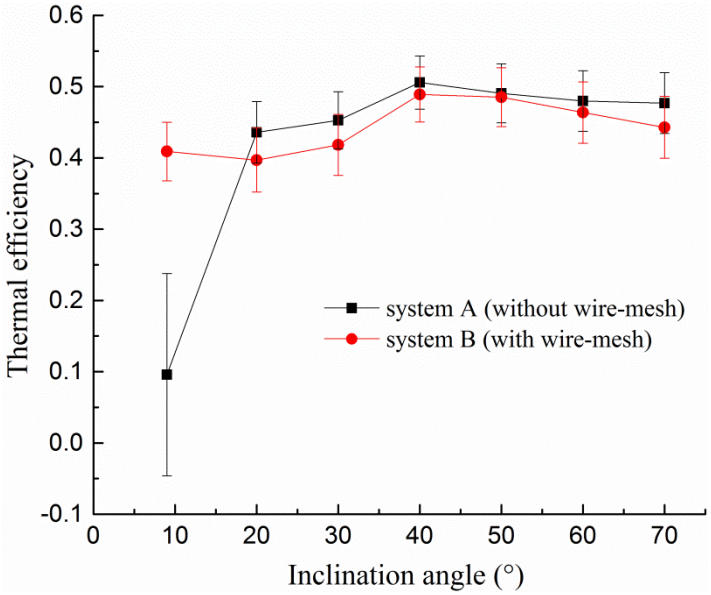

Fig. 9. Thermal efficiency of system A (wickless heat pipe PV/T system) and system B (wire-meshed heat pipe PV/T system).

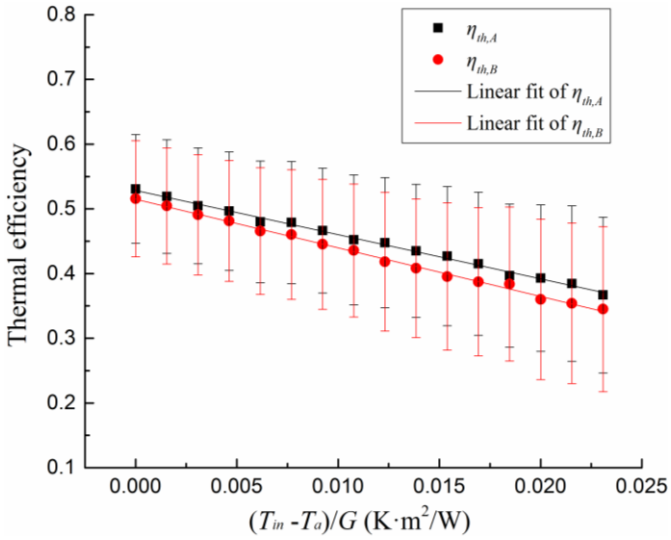

Fig. 10. Instantaneous thermal efficiencies of collector A (wickless heat pipe PV/T collector) and collector B (wire-meshed heat pipe PV/T collector) at an inclination angle of 40°.

Table 1 List of experimental testing and monitoring devices.

Device	Specification	Inaccuracy
Pyranometer	TBQ-2A	±2%
Water flowmeter	LXS 20C	±3%
Power sensor	WBI021S91	±0.5%
Photovoltaic controller	SD4815	/
Thermocouple	Type T (copper-constantan)	±0.5℃
Platinum resistor	PT100	±0.1℃
Data acquisition/switch unit	Agilent 3490A	/